Dissolution of compacted montmorillonite at hyperalkaline pH and 70ºC: *in situ* VSI and *ex situ* AFM measurements

H. SATOH[1],*, T. ISHII[2] AND H. OWADA[2]

[1] *Mitsubishi Materials Corporation, Ibaraki, Japan, and* [2] *Radioactive Waste Management Funding and Research Center, Tokyo, Japan*

ABSTRACT: *In situ* measurements were carried out to quantify montmorillonite dissolution rates at a compaction pressure ranging from 0.04 to 10.00 MPa and temperature of 70ºC in 0.3 M NaOH solution (pH 12.1 at 70ºC) using vertical scanning interferometry (VSI) and an auto-compaction cell. *Ex situ* measurements of the reacted samples using atomic force microscopy (AFM) were performed to quantify the ratio of edge surface area (ESA) to total surface area (TSA) (X_{ESA} = ESA/TSA). Accordingly, the actual ESA for the montmorillonite examined by *in situ* VSI could be estimated. The X_{ESA} value increases as a function of run duration or compaction pressure. At atmospheric pressure, X_{ESA} is approximately 0.0054 and converges to ~0.0107 at 10 MPa, An expression that relates reactive surface area and montmorillonite compaction ($X_{ESA}/X_{ESA\ initial} = kX_{ESA}$, k: variable factor) is $kX_{ESA} = 1.0 + 0.64628P^{0.1527}$ where P is in MPa. Using the calculated X_{ESA}, dissolution rates from the *in situ* VSI measurements are obtained. The early dissolution (<1500 min) at less compaction pressure tends to show faster rates (>1.0×10^{-11} mol/m^2/s) than that at higher compaction pressure. The rates after >1500 min are slower, with values of less than 3×10^{-12} mol/m^2/s, but there is no significant dependency on the density in the range from 1.0 to 1.7 Mg/m^3. These observed rates for compacted montmorillonite are two-orders of magnitude slower (2.63×10^{-13} mol/m^2/s) than dissolution rates in the suspended state.

KEYWORDS: montmorillonite, dissolution, compaction, VSI, AFM, surface area, bentonite buffer, alteration.

To assess the performance of the bentonite barriers that are proposed for use in certain kinds of geological repositories for radioactive-waste, it has become necessary to acquire kinetic data for montmorillonite dissolution under realistic conditions. Previous studies involving batch and flow-through experiments using suspended montmorillonites (Cama *et al.*, 2000; Sato *et al.*, 2004; Rozalen *et al.*, 2008) and monomolecular montmorillonites (Yokoyama *et al.*, 2005; Kuwahara, 2006) have generated dissolution rate data as functions of temperature, solution saturation state and pH. The results have contributed to the estimation of bentonite dissolution rates and the chemical buffering capacity of bentonite. Now, we need to extend the knowledge gained in these experiments to more realistic systems in which bentonite is compacted. However, there are few studies of mineral dissolution under compaction (e.g. Nakayama *et al.*, 2004).

A bentonite buffer intended to be employed in the engineered barrier system of a geological radioactive waste repository would be compacted to maintain the bentonite's permeability at a very low value.

Nakayama *et al.* (2004) studied alkaline alteration of compacted bentonite (Kunigel V1) with silica additive at a dry weight ratio of 70:30 and with a dry density of 1.60 Mg/m^3. Given the amount of montmorillonite in this bentonite is 50.51 wt.% and a silica additive and other minerals in the bentonite have a density of 2.7 Mg/m^3, the calculated density of the montmorillonite is 0.92 Mg/m^3.

In this study, we conducted *in situ* dissolution experiments at pH 12.1 and 70ºC under a broad range of compaction. The pH and temperature simulate a possible cement-leachate in a repository for transuranic (TRU) waste and were maintained by Yokoyama *et al.* (2005) when making AFM measurements. The dissolution rates obtained were used to propose an expression to account for the compaction effect on montmorillonite dissolution.

EXPERIMENTAL METHODS

The *in situ* measurements were performed using a vertical scanning interferomer (VSI, RSI MM5500) and an auto-compaction cell (Syn-Corporation, PC20-200). The system was improved by use of a Linnik interferometer unit and monochromatic filter (λ = 520 nm). The auto-compaction cell consists of a titanium body, a flange with window and a specimen substrate of CVD (chemical vapour deposition, Fig. 1a) diamond. Compaction pressure can be automatically maintained between the window and the substrate using a free piston connected to a pressure-controlling vessel. This method guarantees direct measurements of ultra-slow rates of mineral volume changes during reaction (Satoh *et al.*, 2007; Van Driessche *et al.*, 2011).
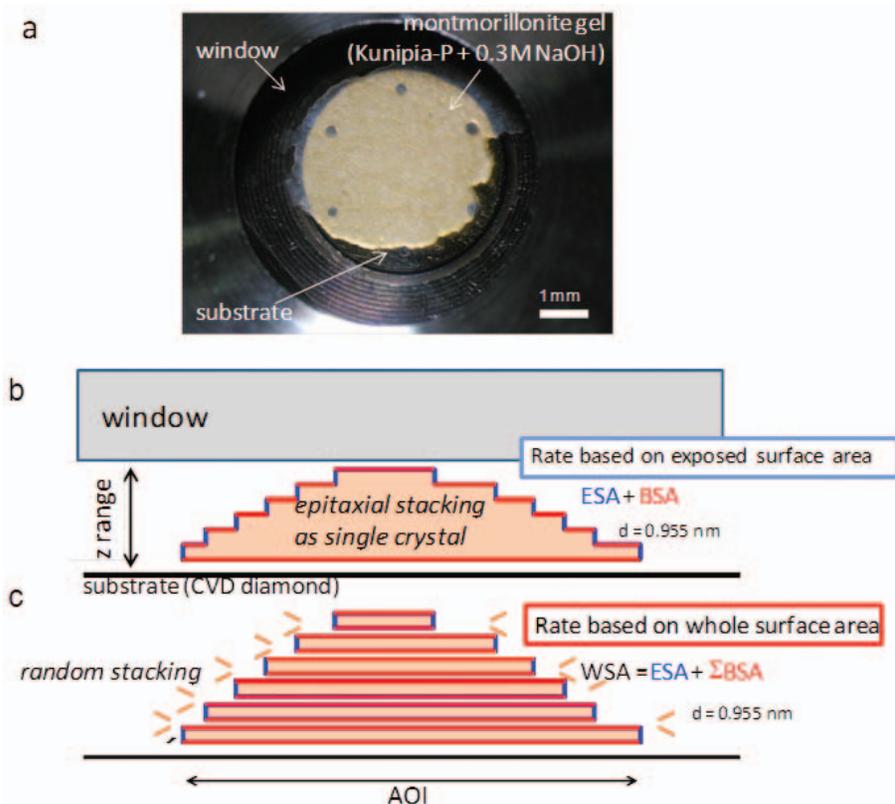

FIG. 1. Specimen in the cell and schematic illustrations showing AFM-assisted surface area analysis and sample specimen. (a) Photomicrograph of starting montmorillonite gel between cell window and substrate with small holes. (b) Conventional *in situ* VSI measurement covering exposed surface area as like single crystal. (c) Novel method to estimate whole surface area (WSA) by integrating every edge (ESA) and basal surface of each interlayer slice at every d = 0.955 nm (ΣBSA), because a montmorillonite gel specimen is a randomly stacked phase.

In situ VSI can only detect changes in the optical path as a relative phase difference, $\Delta I/I_{max}$ of the phase intensity at a wavelength (λ), and refractive index of solution (n). Changes of ΔI with time (Δt) allow the obtainment of mineral dissolution rates: (Rate, mol/m^2/s) using the mineral molar volume (v_m, m^3/mol) (e.g. Satoh *et al.*, 2007):

$$\text{Rate} = \frac{\Delta I}{I_{max}} \times \frac{\lambda}{2 \times n} \times \frac{1}{v_m \times \Delta t} \quad (1)$$

In the case of montmorillonite, an adequate interferogram cannot be obtained directly from the surface in contact with solution because the reflectivity of montmorillonite in solution is weak, probably due to its rough surface and high transmittance. However, satisfactory interferograms can be obtained easily from back-reflected light from the substrate surface of gold-coated diamond (Fig. 1a). This is the same as the interferometric method applied for solution n measurements. Montmorillonite can be assumed to be a higher-n solution, so that the phase intensity of the interferogram through montmorillonite (I_m) of thickness of z ($I_m/I_{max} = 2zn_{mont}/\lambda$) is greater than that in solution of same thickness ($I/I_{max} = 2zn/\lambda$). Therefore, the phase difference can be expressed as $\Delta I/I_{max} = (I - I_m)/I_{max} = 2z(n - n_m)/\lambda$. Finally, the thickness can be calculated to be $z = \Delta I/I_{max} \times \lambda/[2(n - n_m)]$. Then the dissolution rate can be calculated:

$$\text{Rate} = \frac{\Delta I}{I_{max}} \times \frac{\lambda}{2(n - n_m)} \times \frac{1}{v_m \Delta t} \quad (2)$$

where n_m was experimentally determined for Kunipia-P (Kunimine Industry Co.) and equals 1.5003. However, the surface of compacted montmorillonite that is covered with numerous steps is too rough to be measured by interferometry. Optical measurements cannot laterally resolve narrow intersteps and kinked step-edges which are shorter than the wavelength used. The roughness of montmorillonite surfaces causes serious errors in the determined rates.

Dissolution runs were performed using Kunipia-P montmorillonite $(Na_{0.78}K_{0.02}Ca_{0.12})$ $(Al_{3.12}Mg_{0.66}Fe_{0.18}Ti_{0.02})(Si_{7.74}Al_{0.26})O_{20}(OH)_4$; based on O = 22; Yokoyama *et al.*, 2005; molar volume of 272.82×10^{-6} mol/m^3) at compaction pressures in the range $0.04-10.0$ MPa and a temperature of 70ºC in 0.3 M NaOH solution (pH 12.1 at 70ºC). Prior to each run, ~50 µl of starting montmorillonite gel in the same solution (~60 mg/ml) was transferred onto a diamond substrate and quickly bound with a diamond window (Fig. 1a). Then, an HPLC pump was used to supply a solution via a PEEK capillary at a constant rate of 10 µl/min. Effluent solutions were collected in sampler tubes and analysed by ICP-AES. However, since the cell contains a very small amount of montmorillonite (~ 3 mg), the Si and Al concentrations were always below their detection limit (<0.1 ppm). Time-lapse *in situ* VSI measurements were performed with an interval time of 60 s (Δt). Using the measured quantity of montmorillonite (mol) and its volume estimated from the height range and the area of the field of view (235×176 µm^2, 640×480 pixel^2), we calculated the density at each compaction pressure. The results ranged from 1.07 at atmospheric pressure to 1.66 at 10.0 MPa.

EX SITU AFM MEASUREMENTS

It is generally accepted that smectite dissolution takes place at step edges of $\{hk0\}$ faces. Therefore, smectite dissolution rates should be normalized using the edge surface area (ESA) value instead of the total surface area (TSA), which is the sum of the basal surface area (BSA) and edge surface area (ESA) (TSA = BSA + ESA, Yokoyama *et al.*, 2005; Kuwahara, 2007). Owing to the insufficient lateral resolution of VSI, a Veeco Nanoscope III with silicon nitride cantilever in contact mode was used to obtain the required surface area data. After the *in situ* VSI measurements, the reacted samples were individually transferred from the cell into pure water and prepared for *ex situ* AFM observation. The prepared suspensions were deionized with ionic exchange resin and drop-dried on substrates of flat mica $\{001\}$ to improve the image quality, because remaining electrolytes crystallize on mica surfaces and sometimes prevent particle observation. This pure water treatment is very effective to achieve flat and well-dispersed mounts of particles on a mica substrate. We selected particles randomly in several AFM images. Sometimes, during the drying process particles form an overlapped aggregate in several layers. However, the AFM height image can resolve each grain by different contrasts in the image, which indicate the number of monolayers (d_{001}).

Based on the measured ESA ratio (X_{ESA} = ESA/TSA), the actual ESA measured in the *in-situ*

VSI measurements with compacted montmorillonite was used to normalize the dissolution rates. The largest surface area measured by VSI includes the total BSA and the total ESA of layers that compose the scanned surface. This maximum area, namely whole surface area (WSA), can be obtained by adding the BSA of every monomolecular layer, using $d_{001} = 0.955$ nm (Yokoyama *et al.*, 2005) to the small optically detected height change at edges in the area of interest (AOI). Therefore, if X_{ESA} is approximately constant during the measurements, it is possible to estimate ESA for compacted montmorillonite in the field of view, according to the following expression:

$$\text{Rate} = \frac{\sum_{m,n} \Delta I(x_m, y_n)}{I_{max}} \times$$

$$\frac{\lambda}{2(n - n_{smec})} \times \frac{\text{AOI}}{v_m \times \text{WSA} \times X_{ESA} \times \Delta t} \quad (3)$$

where λ is the wavelength (520 nm), n is the refractive index of the solution (1.329244), AOI is the projection area of interest, and v_m is the molar volume of montmorillonite. In this study, the minimum pixel area is 367×367 nm^2. This rate calculation was automatically performed with an SPIP (Image Metrology Co.) and an extended tool, SPIP-EX (M. Yokomine, pers. comm.).

RESULTS AND DISCUSSION

The image data obtained by *in situ* VSI measurements were converted into the molar densities of AOIs (mol/m^2) and the rates (mol/m^2/s). Then the relationships among the rates (mol/m^2/s), compaction pressures (MPa) and densities (g/cm^3) were evaluated. Figure 2a and b show an example VSI snapshot at 8.0 MPa compaction and the inhomogeneous mass distribution of montmorillonite gel in 3-D. Figure 2c shows a plot of temporal variation *vs.* molar density at an AOI (white box) corresponding to a very slow calculated dissolution rate (after X_{ESA} correction, see text below). After each run montmorillonite was recovered from the cell and used for AFM observation. The AFM images showed dissolution and fragmentation signatures on montmorillonite particles (Fig. 3). Two types of etch pits were recognized. One is a linear etch pit due to edge dislocation (Fig. 3b) and the other is an isolated etch pit (Fig. 3c) previously observed by AFM (Yokoyama *et al.*, 2005). The former could have been generated by mechanical
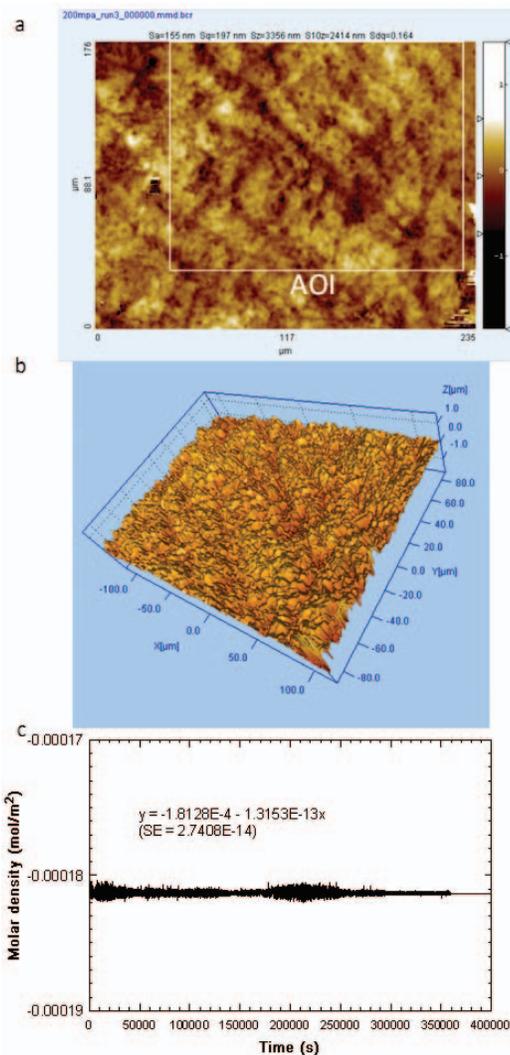

FIG. 2. Measurement of dissolution rate by VSI. (a) A VSI snapshot and analysed AOI at 8.0 MPa. (b) 3-D plot of VSI image. (c) Plot obtained of time (*s*) *vs.* molar density (mol/m^2) at AOI based on actual X_{ESA}. The SE in the plot is standard error (±) of slope by linear regression.

processes such as random-stacking and bending. Completion of linear etching along the grain causes grain separation (fragmentation). The latter originates from point defects or spiral dislocations which could have occurred during the crystal growth process. Fine particles were recognized to have different shapes to those of particles of the initial montmorillonite. These fine particles could be an as
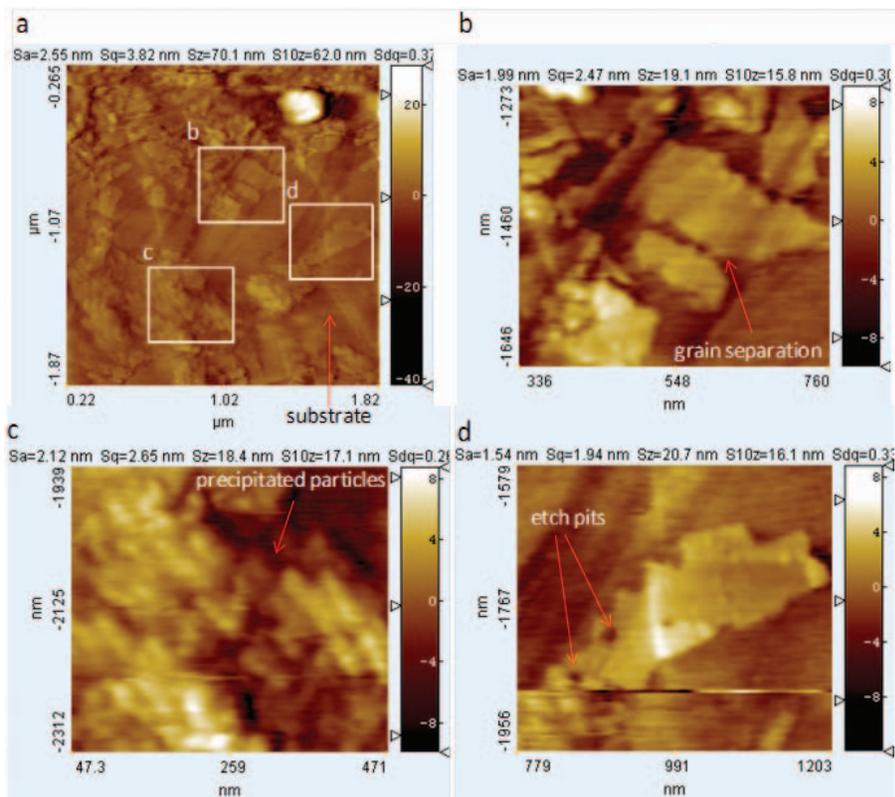
F_{IG}. 3. Evidence of fragmentation of montmorillonite particles observed by AFM: (a) Height image of montmorillonite on a CVD diamond window after run at 10.0 MPa (with white boxes of zoomed images for b, c and d). (b) Image showing fragmentation along edge dislocation. (c) Precipitated particle-like objects. (d) Isolated etch pits.

yet unidentified secondary phase having $d = 1.08$ nm (Fig. 3c).

Mono-molecular grains of up to 200 particles were measured by AFM. Areas and perimeters of particles in the AFM deflection images were individually measured by image processing software (Image J). The median values of the analysed particle areas and perimeters correspond respectively to BSA/2 directly and ESA multiplied by $d = 0.955$ nm. As shown in Fig. 4a and b, observed ESA and also BSA values have wide variations which could have resulted from inhomogeneous reaction in the compacted system. In this study, we adopted the median of the AFM data as being representative of BSA, ESA and TSA. Table 1 summarizes the results of AFM particle analysis by giving representative BSA, ESA, TSA and X_{ESA} values for the VSI runs. The TSA and ESA determined for the starting montmorillonite were

775.6 and 4.2 m^2/g which are sufficiently close to those reported for Kunipia-P by Yokoyama *et al.* (2005). The run for low compaction at 0.04 MPa shows a small ESA peak at 0.0035 µm^2 (Fig. 4a) and large particle size (Fig. 4c), whereas the high compaction run at 10.00 MPa reduces this peak (Fig. 4b) and particle size (Fig. 4c). Assuming a particle is disk shaped, the median diameters for each run were calculated to range from 303 to 231 nm (Fig. 4c). If these size decreases have been caused by dissolution, differences in particle diameter (ΔD) can be used to calculate the dissolution rates:

$$\text{Rate} = \frac{\Delta D}{2} \times \frac{1}{v_m \Delta t} \qquad (4)$$

This calculation gave rates ranging from -3.0^{-11} to 9.1×10^{-10} mol/m^2/s (Table 1), which are faster
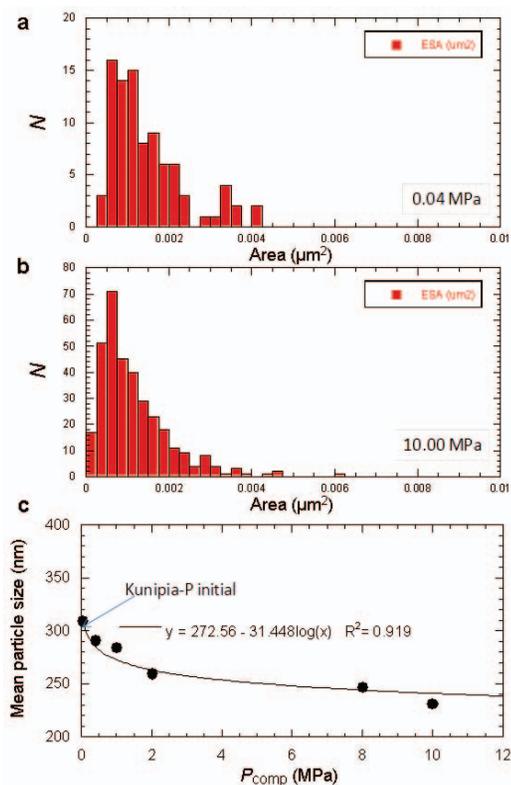
FIG. 4. Results of AFM particle analyses: (a) distribution of edge surface area (ESA) of grains at 0.04 MPa; (b) at 10.00 MPa; (c) change of calculated mean particle size as a function of compaction pressure.

that the rate estimated for the dissolution of a montmorillonite suspension by Sato *et al.* (2004). The faster rate in the present study may not have reflected dissolution but rather fragmentation. Therefore, it is difficult to evaluate the dissolution rate for the compacted system by *ex situ* AFM measurements when the particles may be fragmented.

The X_{ESA} value increases as a function of run duration or compaction pressure. At atmospheric pressure, X_{ESA} is ~0.0054, while at 10 MPa, the X_{ESA} converges to ~0.0107. Using the results, the ratio of $X_{ESA}/X_{ESA\ initial}$ (= kX_{ESA}, k: variable factor) can be formulated as a function of P (MPa) as follows: $kX_{ESA} = 1.0 + 0.64628P^{0.1527}$ (Fig. 5). The density curve as a function of compaction P is shown in Fig. 6. Two different curves were obtained from successive compaction runs on the same montmorillonite and successive compaction runs on an individual montmorillonite sample. This result suggests that during this experiment the compaction was not static but a dynamic process.

The VSI-measured rates based on X_{ESA} by AFM are plotted against the VSI-measured dry density (Fig. 7). Over all compaction runs (0.04−10.0 MPa), early dissolution (<1500 min) at less compaction pressure tends to show faster rates ($>1.0 \times 10^{-11}$ mol/m^2/s) than that at higher compaction pressure (Fig. 7, Table 2). Generally, minerals are dissolved faster at early stages than at later stages because, compared to a sample at later stages, the prepared starting powder or cleaved specimen has larger reactive surfaces which consist of numerous steps and kinks (e.g. Arvidson *et al.*, 2003). Although the VSI data showed a wide range

TABLE 1. Result of *ex situ* AFM grain analysis.

P_{comp} (MPa)	Time (min)	BSA (m^2/g)	ESA (m^2/g)	TSA (m^2/g)	X_{ESA}*	kX_{ESA}	ϕ (nm)**	Rate*** (mol/m^2/s)
10.00	6207	770.59	8.31	778.90	0.010669	1.964112	231.2	0.00E+00
8.00	9955	771.04	7.51	778.56	0.009652	1.776903	247.2	0.00E+00
2.00	7769	768.62	7.95	776.57	0.010237	1.884456	259.8	0.00E+00
1.00	2658	768.61	6.78	775.40	0.008750	1.610730	284.3	0.00E+00
0.40	2455	768.42	6.28	774.70	0.008057	1.483167	291.0	0.00E+00
0.04	6180	768.31	5.92	774.23	0.007642	1.406907	309.0	0.00E+00
0.00	0	775.64	4.24	779.88	0.005432	1.000000	303.0	

* X_{ESA} = ESA/TSA
** grain size is diamter calculated from BSA/2 assuming round shape.
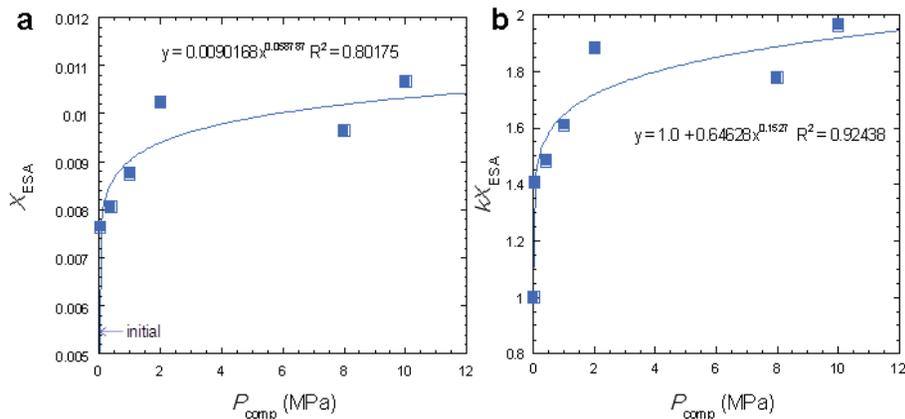*** rate calculated from the change of grain diameter, time and molar volume.

FIG. 5. X_{ESA} (a) and kX_{ESA} (b) as a function of compaction pressure.

in the rates, from 1×10^{-11} to 1×10^{-13} mol/m²/s at 0.04 to 10.00 MPa, all these rates are remarkably slower than those expected for montmorillonite under the same conditions, but without compaction (suspension: 2.93×10^{-11} mol/m²/s; Sato *et al.*, 2004). In this study, the density range covered a smaller range (1.0 to 1.7 Mg/m³), and the rates after >1500 min were slower ($< 3 \times 10^{-12}$ mol/m²/s) but showed no significant dependency on the density. Only the rate variations at the same compaction pressure may be correlated with the density. Particle analyses of montmorillonite at 10. 0 MPa showed a slight increase in smaller particles and decrease in

larger particles, which could be attributed to the increased X_{ESA} by fragmentation. In spite of such an X_{ESA} increase, the dissolution rates were nevertheless reduced.

This rate reduction is more likely to be explained by the limited fluid flow on the nanopore scale, thereby allowing dissolution of surrounding grains to maintain the pore solution close to equilibrium. However, this situation is always in competition with stress-induced dissolution (edge-dislocation, etch pit formation and fragmentation) and growth. The estimated chemical potential for pressure solution (De Meer & Spiers, 1999) implies that
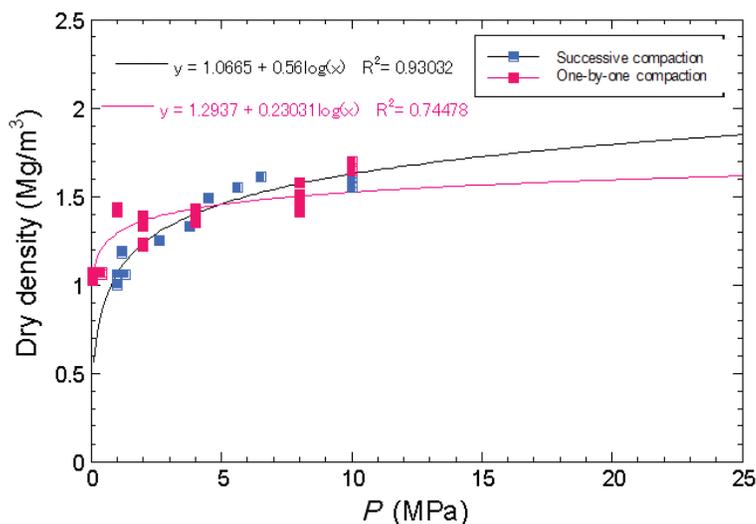

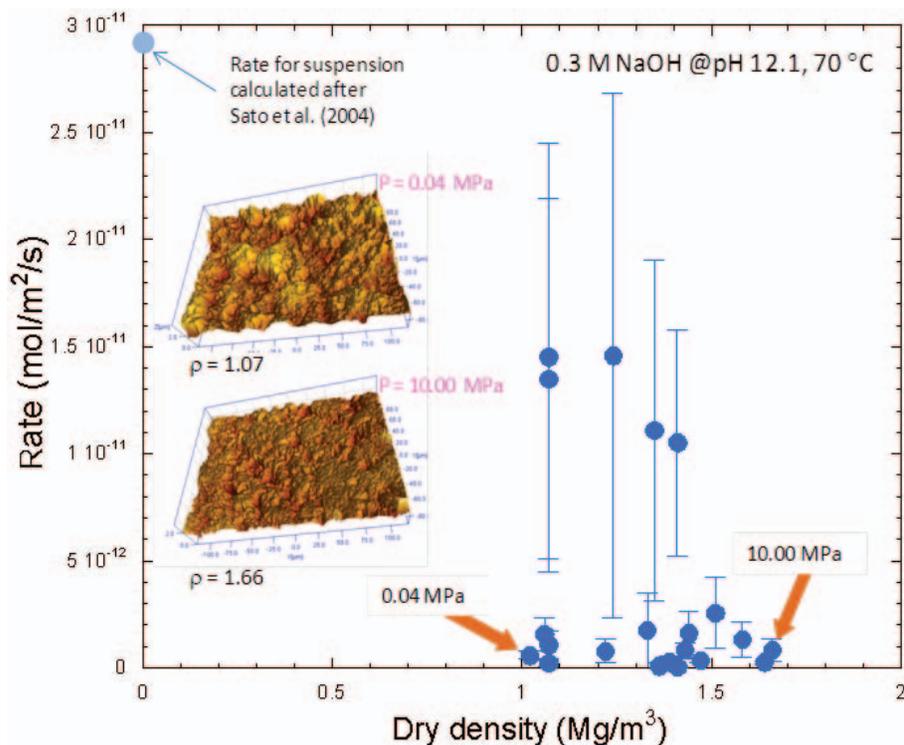FIG. 6. Compaction (*P*) *vs.* dry density measured by *in situ* VSI.

Fig. 7. Plot of dry density *vs.* rate at 0.04 to 10.00 MPa compaction. Imposed 3-D plots are snap shots of *in situ* VSI measurements at $P = 0.04$ and 10.0 MPa. Error bars are defined as standard error of linear regression in the plots of time *vs.* molar density. Faster rates with larger error bars were obtained from early measurements (<1500 min). One point plotted at zero dry density is calculated rate from a kinetic equation for suspended montmorillonite proposed by Sato *et al.* (2004).

the compacted porous media should have either enhanced or reduced chemical potentials for the mineral-fluid system (Fig. 8). A systematic decrease in chemical potential is directly caused by the pressure gradient from the solid to the fluid (= $P - P_f$), and an increase in chemical potential (saturation) is caused by the Gibbs-Thomson effect at curved (roughed) material surfaces surrounding a pore. In our *in situ* VSI experiments, the curvature radius (r_s) was assumed to be only for the vertical section (step density, but for lateral section as kink density) estimated from the VSI measured S_{dq} (root mean square of slope) and d_{001} of montmorillonite (0.955 nm).

TABLE 2. Comparison of dissolution rates between suspended and compacted montmorillonites.

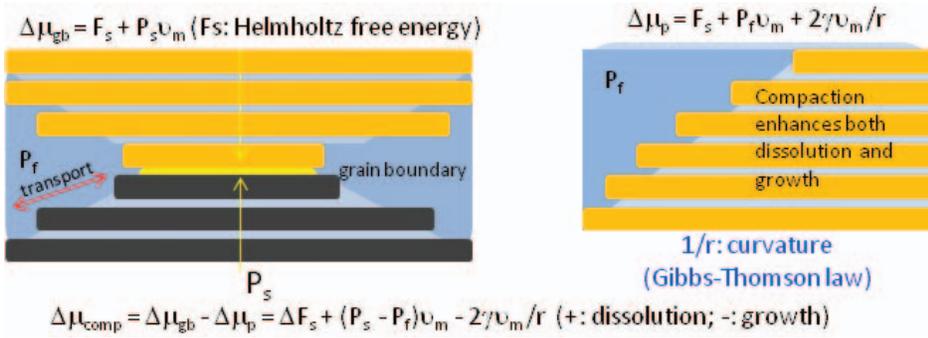| Montmorillonite state	Pressure (MPa)	Density	Rate (mol/m^2/s)	Literature
Compacted (early)	0.04	1.02	1.45E-11	This study
Compacted (>1500 min)	0.04	1.02	5.89E-13	do.
Compacted (early)	10.0	1.66	8.55E-13	do.
Compacted (>1500 min)	10.0	1.64	2.64E-13	do.
Suspended		0.001	2.93E-11	Sato *et al.* (2004)

FIG. 8. Sketches illustrating chemical potential for compacted mineral-fluid system: (a, left) chemical potential involving Helmholtz free energy for grain boundary in pore fluid; (b, right) chemical potential involving Gibbs-Thomson effect for pore fluid near grain surface.

$$r_s = d_{001} + \frac{d_{001}}{S_{dq}^2} \qquad (5)$$

This radius (r_s) and the interfacial energy between montmorillonite and alkaline solution (γ) determine the Gibbs-Thomson effect. The interfacial energy was calculated to be 43.4 mJ/m^2 by means of a wetting-angle measurement (Giese *et*
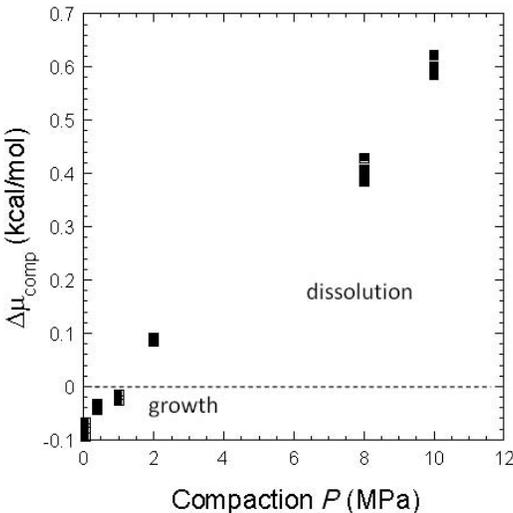

FIG. 9. Compaction pressure *vs.* calculated chemical potential. Compaction pressure less than 1.5 MPa represents small saturation (growth), but compaction pressure greater than 1.5 MPa enhances undersaturation (dissolution). Note that these estimated potentials are small, only <1.0 kcal/mol under the experimented pressure less than 10.00 MPa.

al., 1991). The change in chemical potential for the compacted system, $\Delta\mu_{comp}$, can be denoted simply by the Gibbs-Thomson effect, pressure gradient from solid to fluid and molar volume of the solid (υ_m). So, the overall chemical potential ($\Delta Gr'$) can be expressed as follows:

$$\Delta Gr' = \Delta Gr - \Delta\mu_{comp}$$
$$= \Delta Gr - (P - P_f) \cdot \upsilon_m + \frac{2\gamma\upsilon_m}{r_s} \qquad (6)$$

However, as shown in Fig. 9, the calculated changes in chemical potential by compaction were found to be negligibly small for our experiments (-1.0 to $+0.6$ kcal/mol). It is suggested that strong compaction nevertheless keeps the system undersaturated, so that dissolution could have indeed been detected in our experiments.

As a significant effect other than chemical potential, we finally focus on the variable surface area for the compacted system. Our AFM investigation revealed the variable ESA as a function of compaction pressure (Fig. 5). As already mentioned, the effective surface area of montmorillonite as a function of pressure, $A_{min}(P)$ can be empirically formulated as follows:

$$A_{min}(P) = (1.0 + 0.64628 \cdot P^{0.1527}) \cdot A_{min} \qquad (7)$$

where A_{min} is the initial ESA before compaction. However, as shown in Fig. 5b, $A_{min}(P)$ is not so intensive because kX_{ESA} decreases below 2 only at 10.0 MPa.

We still need to consider the other important effect by really exposed surfaces in the compacted

system. The most remarkable difference between the suspended and compacted states of montmorillonite is the pore spacing. This difference can possibly be investigated numerically (e.g. Dijkstra *et al.*, 1997) or geometrically. Such approaches may improve the $A_{\min}(P)$ thereby allowing more realistic behaviour to be reproduced. The improved function, $A_{\min}(P)$ may be able to predict the dissolution rate of compacted motmorillonite caused by the variation in exposed surface area during compaction.

SUMMARY AND CONCLUSIONS

Using *in situ* VSI and *ex situ* AFM measurements, we measured the dissolution rates of compacted montmorillonite at hyperalkaline pH and 70ºC under pressures ranging from 0.04 to 10.00 MPa. The observed dissolution rates were $1-2$ orders of magnitude slower than those expected for suspended montmorillonite under the same conditions. This rate reduction can be explained by limited water flow in the nanopores in which the dissolution of surrounding grains takes place. Consequently, the pore solution approaches equilibrium. Owing to pressure solution, compacted porous media should have either enhanced or reduced chemical potentials for the mineral–fluid system. However, the calculated changes in chemical potentials due to compaction of bentonite were found to be negligible in our experiments (-1.0 to $+0.6$ kcal/mol). The effective surface area of montmorillonite as a function of pressure, $A_{\min}(P)$ may be able to predict the dissolution rate of compacted montmorillonite during compaction due to the variable exposed surface area.

In this study, we revealed experimentally that compaction can destabilize montmorillonite grains physically, but stabilize the bentonite system chemically.

REFERENCES

Arvidson R.S., Ertan I.E., Amonette J. E. & Lüttge A. (2003) Rates of calcite dissolution obtained by vertical scanning interferometry. *Geochimica et Cosmochimica Acta*, **67**, 1623−1634.

Cama J., Ganor J., Ayora C. & Lasaga A.C. (2000) Smectite dissolution kinetics at 80ºC and pH 8.8. *Geochimica et Cosmochimica Acta*, **64**, 2701−2717.

De Meer S. & Spiers C.J. (1999) On mechanisms and kinetics of creep by intergranular pressure solution. Pp. 345−366 in: *Growth, Dissolution and Pattern Formation in Geosystems* (B. Jamtveit & P. Meakin, editors). Kluwer Academic Publishers.

Dijkstra M., Hansen J.-P., & Madden P.A. (1997) Statistical model for the structure and gelation of smectite clay suspensions. *Physical Review E*, **55**, 3044−3053.

Giese R.F., Costanzo P.M. & van Oss C.J. (1991) The surface free energies of talc and pyrophyllite. *Physics and Chemistry of Min*erals, **17**, 611−616.

Kuwahara Y. (2006) In-situ AFM study of smectite dissolution under alkaline conditions at room temperature. *American Mineralogist*, **91**, 1142−1149.

Nakayama S., Sakamoto Y., Yamaguchi T., Akai M., Tanaka T., Sato T. & Iida Y. (2004) Dissolution of montmorillonite in compacted bentonite by highly alkaline aqueous solutions and diffusivity of hydroxide ions. *Applied Clay Sci*ence, **27**, 53−65.

Rozalén M.L., Huertas F.J., Brady P.V., Cama J., García-Palma S. & Linares J. (2008) Experimental study of the effect of pH on the kinetics of montmorillonite dissolution at 25ºC. *Geochimica et Cosmochimica Acta*, **72**, 4224−4253.

Sato T., Kuroda M., Yokoyama S., Tsutsui M., Fukushi K., Tanaka T. & Makayama S. (2004) Dissolution mechanism and kinetics of smectite under alkaline conditions. *Proceedings of the Internations Workshop on Bentonite−Cement Interaction in Repository Environments*, A3, 38−41.

Satoh H., Nishimura Y., Tsukamoto K., Ueda A., Kato K. & Ueta S. (2007) In-situ measurement of dissolution of anorthite in Na-Cl-OH solutions at 22ºC using phase-shift interferometry. *American Mineralogist*, **92**, 503−509.

Van Driessche A.E.S., García-Ruíz J.M., Tsukamoto K., Patiño-Lopez L.D. & Satoh H. (2011) Ultraslow growth rates of giant gypsum crystals. *PNAS*, **108**, 15721−15726.

Yokoyama S., Kuroda M. & Sato T. (2005) Atomic force microscopy study of mintmorillonite dissolution under highly alkaline conditions. *Clays and Clay Minerals*, **53**, 147−154.